IEEE Photonics Journal
An IEEE Photonics Society Publication

Open Access

Ultra-Broadband Mode Converter Using Cascading Chirped Long-Period Fiber Grating

Volume 11, Number 6, December 2019

Mao Feng
Yange Liu
Zhi Wang
Baiwei Mao
Hongwei Zhang

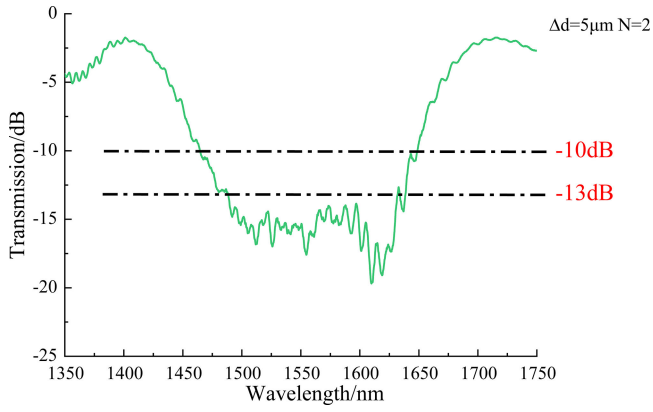

DOI: 10.1109/JPHOT.2019.2951389

Ultra-Broadband Mode Converter Using Cascading Chirped Long-Period Fiber Grating

Mao Feng, Yange Liu, Zhi Wang, Baiwei Mao, and Hongwei Zhang

Tianjin Key Laboratory of Optoelectronic Sensor and Sensing Network Technology, and Institute of Modern Optics, Nankai University, Tianjin 300071, China

DOI:10.1109/JPHOT.2019.2951389

Manuscript received September 20, 2019; revised October 14, 2019; accepted October 31, 2019. Date of publication November 4, 2019; date of current version December 16, 2019. This work was jointly supported by the National Key R&D Program of China under Grants 2018YFB1801802, 2018YFB0504401, and 2018YFB070, the National Natural Science Foundation of China under Grants 61835006, 11674177, 61775107, and 11704283, and the 111 Project under Grant B16027. Corresponding author: Yange Liu (e-mail: ygliu@nankai.edu.cn).

Abstract: We propose and demonstrate an ultra-broadband mode converter based on a cascade chirped long-period fiber grating (CLPFG) written in a two-mode fiber. The mode converter can convert fundamental mode (HE_{11}^{even} and HE_{11}^{odd} modes) into the first order cylindrical vector (CV) modes (TE_{01}, TM_{01}, HE_{21}^{even} and HE_{21}^{odd} modes). We design and analyze the mode conversion characteristics of this kind of grating in theory. The simulation results show a 10 dB bandwidth of 170 nm and 20 dB bandwidth of 145 nm can be achieved by optimizing the parameters of the CLPFG. In the terms of experiment, we achieve the broadband mode converter with 10 dB bandwidth of 170 nm from 1472 nm to 1642 nm.

Index Terms: Long-period fiber grating, cylindrical vector mode, mode converter, ultra-broadband.

1. Introduction

Mode-Division multiplexing (MDM) system, which uses different modes in a few-mode fiber (FMF) as independent channels to transfer different information, has a great potential in expanding the transmission capacity in communication system [1]–[7]. And the mode converter is a key device to transfer the fundamental mode to a higher order one in a MDM system. Generally speaking, mode converters contain spatial devices [8], waveguides [9]–[12] and all-fiber devices [13]–[17]. Compared with spatial devices, all-fiber devices, such as mode-selective couplers and fiber gratings, have the advantages of simpler structure, lower insert loss and easier to integrate with fiber systems, which has become an excellent choice for fiber communication systems. Compared with the mode selective coupler, the fiber grating is simpler in structure and less difficult to manufacture, so it is a better choice as mode converter.

However, generally speaking, normal fiber grating used as mode converter only has dozens of nanometers' narrow operating bandwidth, which is a great restriction. For example, Giles *et al.* used long period fiber grating (LPFG) as a mode converter by introducing a mechanical perturbation, the 10 dB bandwidth is around 35 nm and the 20 dB bandwidth is around 10 nm [18]. Han *et al.* proposed a controllable all-fiber converter using a uniform LPFG fabricated by a CO_2 laser, but its 10 dB bandwidth is only 50 nm and the 20 dB bandwidth is less than 10 nm [19]. Zhao *et al.*

fabricated tilted uniform LPFG in a two-mode fiber as mode converter and the 20 dB bandwidth are still less than 30 nm [14].

Many methods have been used both in simulation and experiment to expand the working bandwidth of LPFGs. Dong *et al.* expanded the 20 dB working bandwidth to 34 nm by reducing the number of the grating periods to 15 [20]. Guo *et al.* reduced the number of the grating period to 8 and got a 15 dB operation bandwidth of 76 nm [21]. This is almost the broadest working wavelength range which could be achieved using this method. They then proposed and demonstrated a LPFG with a 15 dB bandwidth of more than 110 nm on account of a dual-resonance coupling mechanism [22]. Ramachandran and his group did a lot of research on the dispersion properties and they fabricated LPFG at turn-around-point to expand working bandwidth [23]–[26]. Through this way, they got a mode converter which has a 20 dB bandwidth (corresponding mode conversion efficiency 99%) over 63 nm [27]. However, this method requires special design of the fiber, otherwise the working band is fixed. Dan *et al.* designed a chirped device to get a 99% (corresponding to 20 dB) working bandwidth of 47 nm at 1090 nm, which is 5.8 times broader than the uniform gratings. Meanwhile, in the experimental part, the bandwidth was improved by a factor of 5.4 times [28]. Ke *et al.* analyzed the phase-shifted LPFG theoretically and the results showed that the phase-shifted LPFG can increase the working bandwidth, but it will sacrifice the conversion efficiency [29]. Yao *et al.* analyzed and optimized the transmission spectra of chirped LPFG and got a 60 nm 10 dB bandwidth in simulation [30]. However, the introduction of chirp in LPFG will cause a reduction in the coupling efficiency, although this method can achieve a broader working bandwidth. Wang *et al.* propose an ultra-broadband mode converter based on the structure of a length-apodized long-period grating fabricated on waveguide and the measured 20 dB bandwidth was about 120 nm [9]. However, the rectangular waveguide structure is difficult to integrate with fiber system. So, getting a broadband mode converter with a high coupling efficiency as well as a low insertion loss in all-fiber system is still challenging.

In this paper, a new kind of chirp and cascading LPFG is proposed. Through designing elaborately the chirp parameters and the number of the cascading grating, a controllable wavelength range over 20 dB modulation depth can be achieved. We analyzed the effect of different parameters on the mode conversion characteristics of the LPFG. Finally, we get an ultra-broadband LPFG both in simulation and experiment. 10 dB bandwidth of the grating is over 170 nm and 20 dB bandwidth is over 140 nm in simulation. And a 10 dB bandwidth of 170 nm from 1472 nm to 1642 nm is achieved in experiment. The four cylindrical vector (CV) modes of LP_{11} mode group could be generated and detected within this band. This kind of mode converter could be used in optical tweezers [31], high-resolution imaging [32], surface plasmon excitation [33], material processing [34] and some other fields.

2. Grating Design

General few-mode fiber satisfies the weak guide condition, so we can solve the electric fields to acquire linearly polarized (LP) modes due to their convenient expression and application [35]. To note that, LP_{01} mode is a superposition of HE_{11}^{even} and HE_{11}^{odd} modes, LP_{11} mode is a superposition of TE_{01}, TM_{01}, HE_{21}^{even} and HE_{21}^{odd} modes. The fiber we used is a kind of two-mode fiber and its core and cladding radius are 9.5 μm and 62.5 μm, respectively. This fiber could support two LP modes (LP_{01} mode and LP_{11} mode) for stable propagation when the wavelength is less than 1.8 μm according to the simulation result on COMSOL multiphysics (based on finite element method, FEM).

According to the phase-matching condition, the relationship between resonance wavelength and the period (Λ) of fiber grating for coupling between LP_{01} and LP_{11} mode could be characterized by the following equation [22]:

$$\Lambda = \frac{\lambda_{res}}{n_{\text{eff,LP}_{01}} - n_{\text{eff,LP}_{11}}}, \tag{1}$$

where the n_{eff} represents the effective refractive index of the mode in fiber. Fig. 1 shows the period versus resonant wavelength of fiber grating for coupling between fundamental mode and first-order

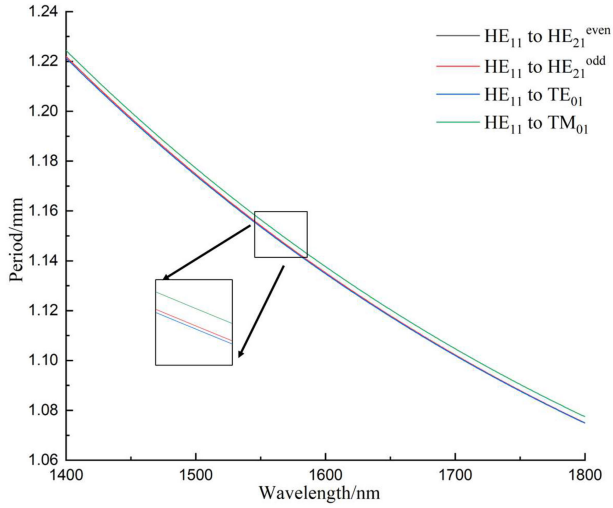

Fig. 1. Period of the LPFG versus different resonant wavelength.

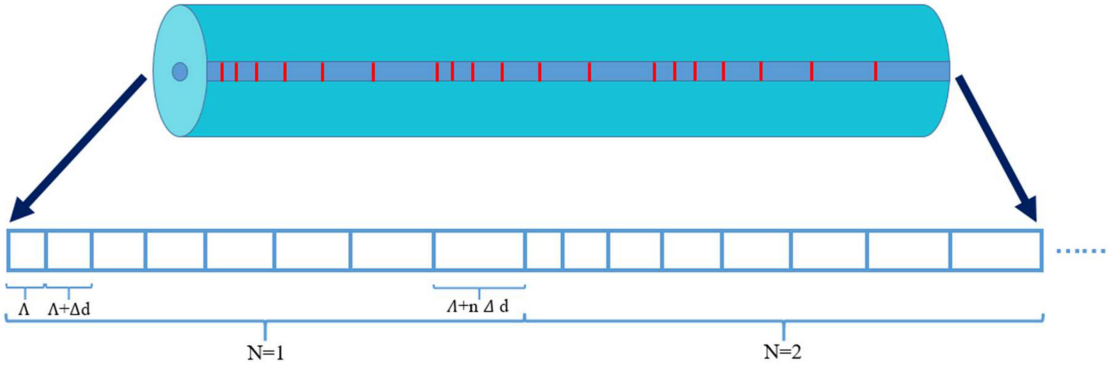

Fig. 2. Profile of the cascade CLPFG.

CV mode. From Fig. 1 we can see that, at the same wavelength, the period difference of fiber grating is very small for the coupling between fundamental and different first-order CV modes. For example, the difference of the period mentioned above is less than 3 μm at 1550 nm. At the same time, refractive index differences among four first-order CV modes is about 0.1% of the difference between fundamental mode and first-order CV mode. In fiber system, the conversion between four CV modes can be realized by introducing a perturbation (such as a polarization controller) [36]. Therefore, we can simplify the four first-order CV mode refractive indexes into an LP_{11} mode refractive index to make the following calculation simpler.

In order to achieve a broadband operation, we introduced a linear chirping into LPFG and cascaded the CLPFG. A schematic diagram is shown in Fig. 2, Δd is used to describe the chirping of the LPFG, and N represents the cascading parameter of the CLPFG. The starting period (Λ) and end period ($\Lambda + n\Delta$d) of the CLPFG is calculated by equation (1). When starting period, end period and Δd are set, the parameter n can be calculated by them. For example, when starting period is 1 mm, end period is 2 mm, Δd is 10 μm, then n will equal to 10.

The energy conversion between two modes in this grating we designed could be described by [37]

$$\begin{pmatrix} L\,P_{01}(z) \\ L\,P_{11}(z) \end{pmatrix} = M_N \ldots M_i \ldots M_1 \begin{pmatrix} L\,P_{01}(0) \\ L\,P_{11}(0) \end{pmatrix}, \tag{2}$$

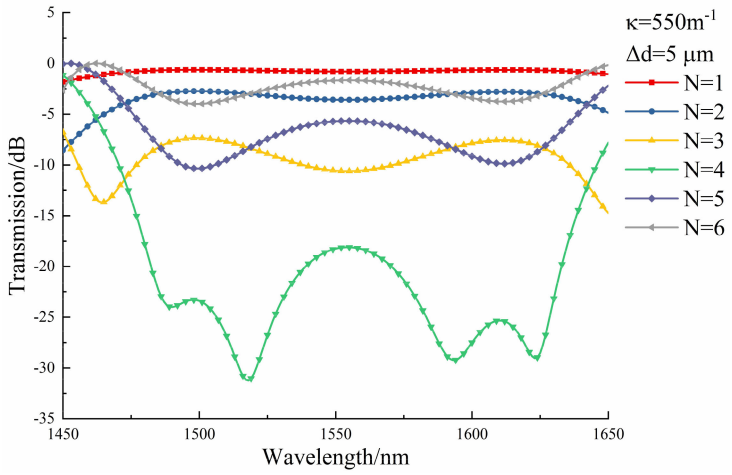

Fig. 3. The transmission spectrum of the demonstrated LPFG when N is increasing.

where the M_i is the transfer matrix for the each CLPFG, and $M_i =$

$$\begin{pmatrix} \cos(\gamma z) + i\frac{\Delta}{\gamma}\sin(\gamma z) & i\frac{\kappa}{\gamma}\sin(\gamma z) \\ i\frac{\kappa}{\gamma}\sin(\gamma z) & \cos(\gamma z) - i\frac{\Delta}{\gamma}\sin(\gamma z) \end{pmatrix}. \tag{3}$$

In equation (3), $\Delta = \frac{1}{2}[\beta_B - (\beta_A + qG)]$ reveals the parameter of phase mismatch, G equals to $2\pi/\Lambda$, and in general, we set the coefficient $q = 1$. Parameter κ represents coupling constant of the fiber grating. Parameter γ is defined by equation $\gamma = \sqrt[2]{\kappa\kappa^* + \Delta^2}$, and z represents the distance in propagation direction. $LP_{01}(0)$ and $LP_{11}(0)$ represent the intensity of incident light, $LP_{01}(z)$ and $LP_{11}(z)$ represent the light beam's intensity at the z-coordinate along the propagation axis, respectively. Usually, we set the input light $LP_{01}(0) = 1$ and $LP_{11}(0) = 0$, which means that only fundamental mode is launched into the LPFG. For a uniform grating, its normalized transmittance can be expressed as [38]–[40]

$$|LP_{01}(z)/LP_{01}(0)|^2 = 1 - \frac{\kappa\kappa^*}{\gamma^2}\sin^2(\gamma z). \tag{4}$$

From equation (4), we can see that for a single uniform grating, its transmission spectrum is mainly determined by coupling constant, length and period of the LPFG. When using the transmission matrix to calculate transmission spectrum of the cascaded CLPFG, we need to segment the chirped grating, and each segment is approximated as a uniform grating. The transmission spectrum of the entire structure is superimposed by these uniform gratings.

According to the simulation result shown in Fig. 1, we set starting period $\Lambda = 1.11$ mm and end period $\Lambda + n\Delta d = 1.2$ mm, which corresponds to the resonant wavelength 1650 nm and 1450 nm, respectively. Firstly, we set coupling constant κ to 550 m^{-1} in order to figure out how the length of grating influences the transmission spectrum. To note that, when coupling constant κ, starting period Λ and end period $\Lambda + n\Delta d$ are set, the length of CLPFG is determined by cascading parameter N and chirped parameter Δd. In Fig. 3, we firstly analyzed the influence of the N when $\Delta d = 5$ μm. We can see the coupling efficiency increases when N is rising from 1 to 4 and get maximum coupling efficiency at $N = 4$. But when N is over 4, the coupling efficiency begins to decrease.

We then set $N = 4$ to analyze the influence of the change in Δd on the transmission spectra. In Fig. 4, we can see when Δd rises from 3 μm to 5 μm, the coupling efficiency increases, while Δd continues to rise, the coupling efficiency will decrease. And from the result we can see that when $N = 4$ and $\Delta d = 5$ μm, we can get the best result that the coupling efficiency is over 20 dB (corresponding to 99%) in a large operation range.

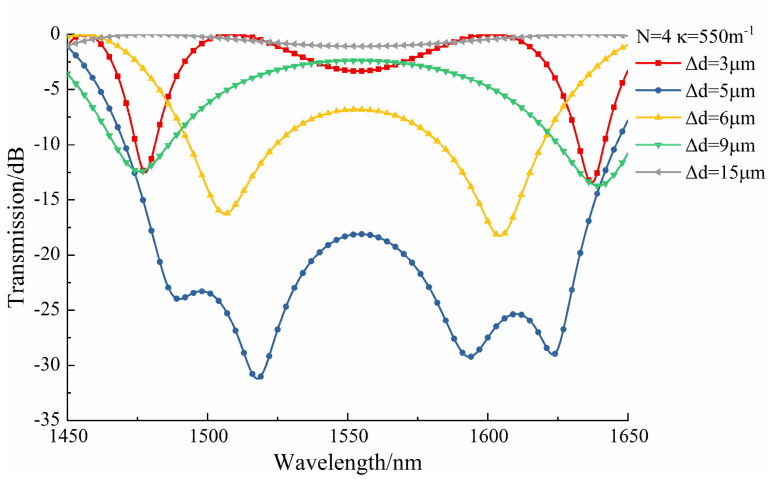

Fig. 4. The transmission spectrum when Δd is changed at the same N.

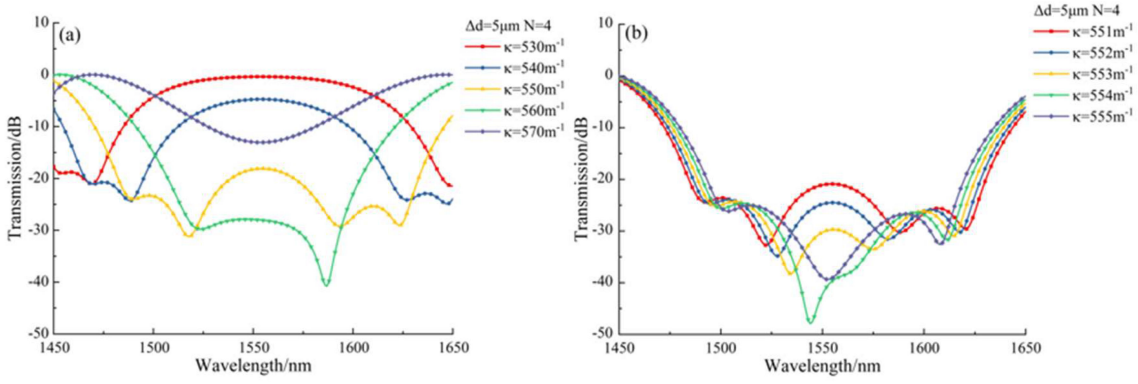

Fig. 5. The transmission spectra when coupling constant is changed while $\Delta d = 5\ \mu m$ and $N = 4$.

After that, we set $\Delta d = 5\ \mu m$, $N = 4$, and change the coupling constant κ to see its influence on transmission spectra. As shown in Fig. 5, we calculated transmission spectra at different coupling constant to search for the best result. Fig. 5(a) is a large-scale adjustment and Fig. 5(b) is a fine-tuned result on the basis of Fig. 5(a). Finally, when coupling constant $\kappa = 551\ m^{-1}$, we get a 20 dB bandwidth of 145 nm from 1485 nm to 1630 nm and its 10 dB bandwidth is 170 nm from 1472 nm to 1642 nm(red curve in Fig. 5(b)).

Considering that if we use the optimized parameters above to fabricate the CLPFG, the total length is about 87.78 mm, which is too long to fabricate. Therefore, we adjust the length of the CLPFG by changing the cascading number N to 2 and optimize the parameter again. At last, we get a 15 dB bandwidth of 102 nm from 1505 nm to 1607 nm, and a 10 dB bandwidth of 129 nm from 1492 nm to 1621 nm when $\Delta d = 5$, $N = 2$ and $\kappa = 521\ m^{-1}$ (shown in Fig. 6).

From the examples we showed above, we can see that we get an ultra-broadband operation range with a high coupling efficiency using the cascade chirped LPFG. Especially, the operation range is controllable by the phase matching condition, which means it could be applied to any band. The feature of transmission spectra has been analyzed clearly and shows a good application potential as a mode converter.

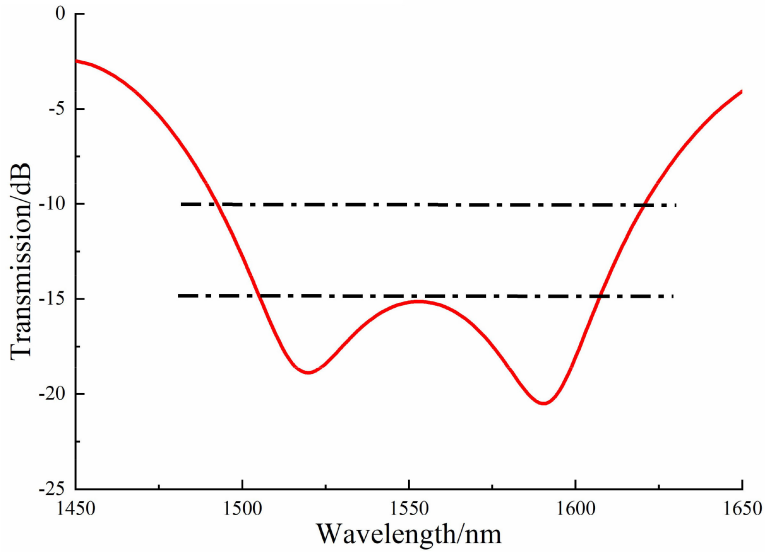

Fig. 6. The transmission spectrum when d = 5, N = 2 and $\kappa = 521\ m^{-1}$.

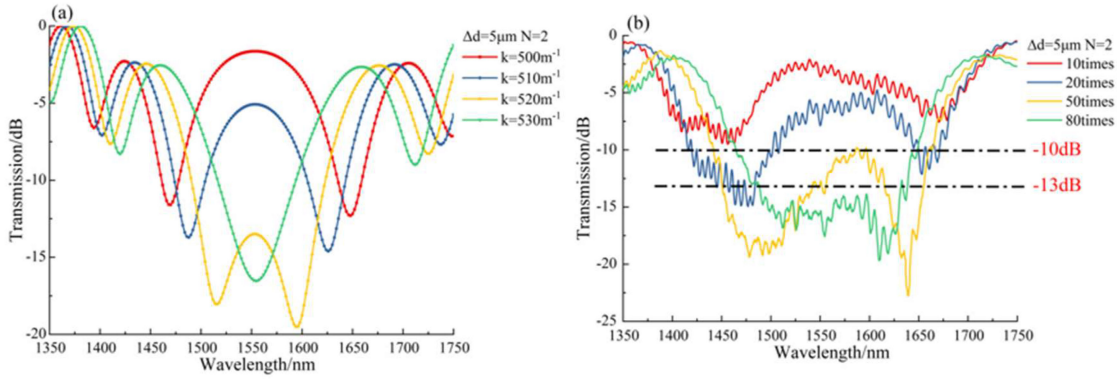

Fig. 7. (a) The transmission spectrum when Δd = 5 μm and N = 2. (b) The corresponding experimental result.

3. Experimental Results and Discussion

In experimental part, we use a CO_2 laser (CO_2-H_30, Han's Laser, the maximum power of laser is 30 W) to fabricate the LPFG we proposed above. At first, light from a supercontinum source launches into the FMF and then passes through a 3 m single mode fiber. After that, an optical spectrum analyzer (OSA, TOKOGAWA, AQ6375) detects the transmission spectrum of the LPFG. We set the output power of CO_2 laser 7% and change the coupling constant κ by change the writing times.

We fabricate the LPFG with different repeated times and make a contrast to the simulation results. From Fig. 7, we can see the spectra with repeated times of 10, 20, 50 and 80 are corresponding to the simulation results when coupling contrasts are fixed at 500 m^{-1}, 510 m^{-1}, 520 m^{-1} and 530 m^{-1}. This means coupling constant could be controlled by changing the repeated times, coupling constant will increase as the repeated times rising. Maximum insertion loss of the LPFG is 1.75 dB and there are many oscillations in the transmission spectra which is mainly caused by intermodal interference. As a result, we can see that when repeated times is 80, the 10 dB bandwidth (whose conversion efficiency is 90%) is 170 nm from 1470 nm to 1640 nm and the 13 dB bandwidth (whose conversion efficiency is 95%) is 145 nm from 1487 nm to 1632 nm, which has

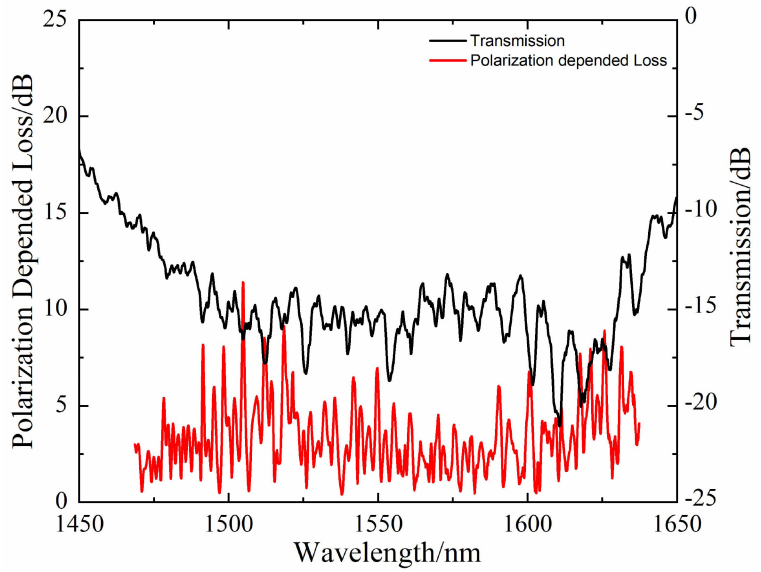

Fig. 8. Transmission spectrum and polarization depended loss spectrum after 80 times' fabrication when $\Delta d = 5\ \mu m$ and $N = 2$.

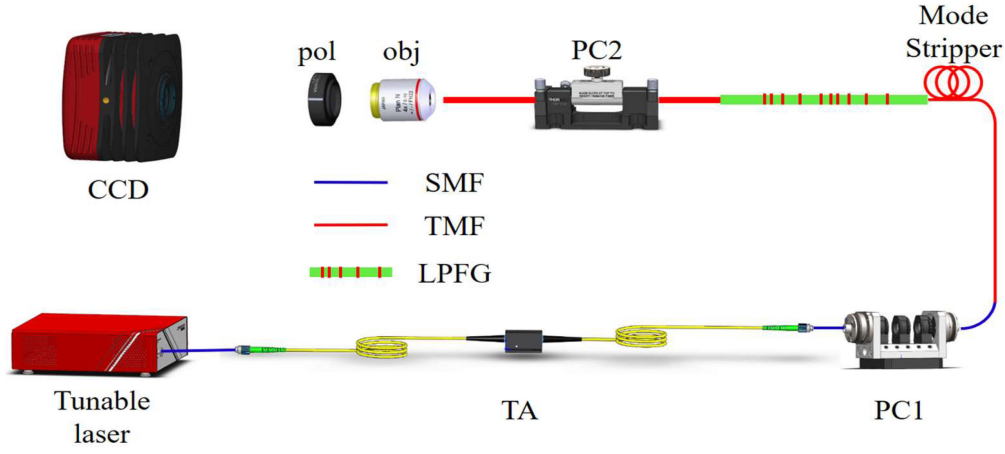

Fig. 9. Experimental set up: pol: polarizer, obj: objective lens, TA: tunable attenuator, SMF: single-mode fiber, TMF: two-mode fiber, PC: polarization controller.

a good agreement with the simulation results. We also measure polarization depended loss (PDL) of the CLPFG in Fig. 8 using a tunable laser and a polarization control system(1454 nm-1640 nm, KEYSIGHT, 8164B, N7786B) [13]. The incident light from tunable laser could be tuned to any polarization state under the control of computer so PDL could be calculated, and the maximum PDL is 11.41 dB at 1504.87 nm. Except for the maximum value, PDL in measured wavelength range is below 10 dB, which is similar to the value of uniform LPFG [14]. PDL is caused mainly by the asymmetrical refractive index modulation due to the asymmetric fabrication, which will lead to a strong birefringence [41]. We can reduce PDL in the future by means of symmetric fabrication or some other ways.

We build detection system shown in Fig. 9 to detect the CV mode converted by the CLPFG we fabricated. Start from the tunable laser, CW laser is first adjusted to an appropriate intensity by a

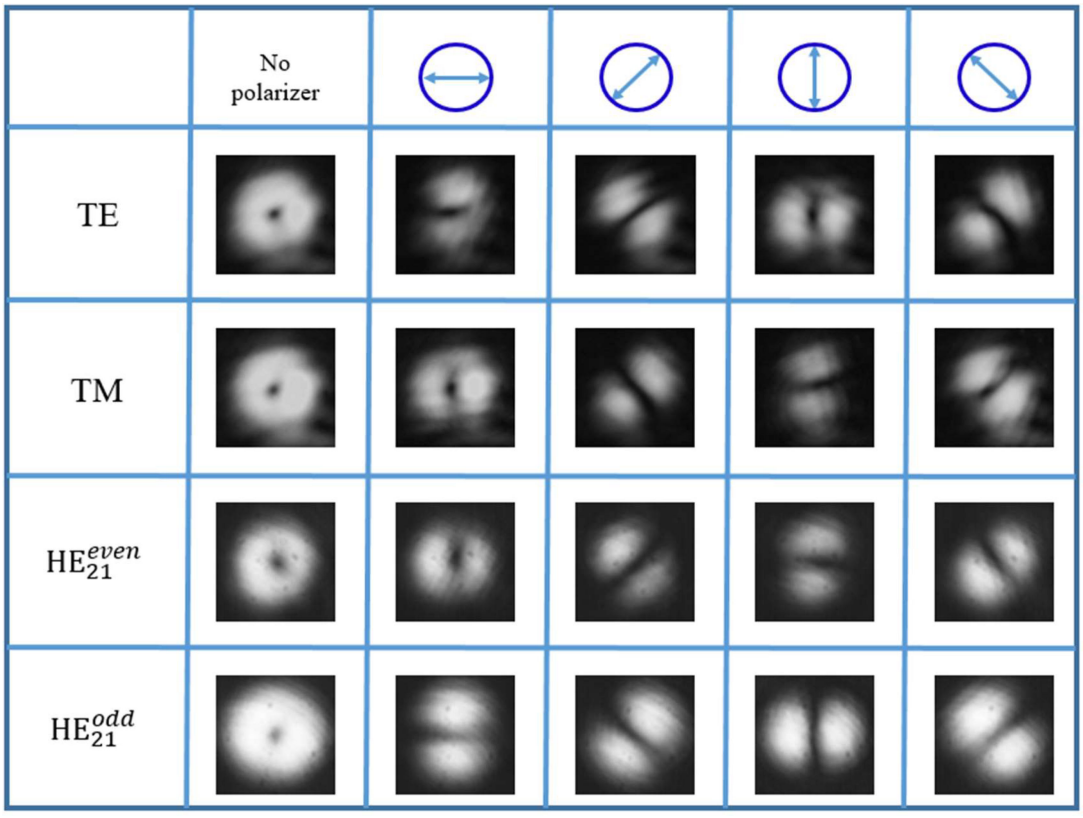

Fig. 10. Intensity profile of the four first order CV modes without polarizer and with different orientations of the linear polarizer at 1564 nm.

tunable attenuator (TA), and then enters a polarization controller (PC1) to adjust the polarization state in order to get the best conversion efficiency. After that, CW laser enters TMF and passes through a mode stripper to ensure only fundamental mode is launched into the CLPFG. Output light of the CLPFG has been converted into first-order CV modes. Then we can get four pure first-order CV modes by adjusting another polarization controller (PC2). An objective lens is used to collimate the output laser from TMF so that the CCD camera could detect the light field distribution conveniently.

By adjusting PC2 to a proper position, TE_{01}, TM_{01}, HE_{21}^{even} and HE_{21}^{odd} modes with doughnut shape could be detected. In order to distinguish which CV mode the doughnut-shaped light field belongs to, we added a polarizer before the output beam is detected by CCD camera and set it at different angles. Fig. 10 shows the field distribution of the four CV modes at 1564 nm. The first vertical row shows the field distribution without polarizer. And the rest rows are the field distribution when we set the polarizer at 0°, 45°, 90°, and 135° (we set the x-axis as the 0°), from which we can judge the four CV modes. In the meantime, we shows the field distribution of HE_{21}^{even} mode at different wavelength in Fig. 11. The other CV modes at these wavelengths can also be detected by adjusting PC2 into a proper position, which shows that the CLPFG we fabricated can achieve a broadband working range.

The proposed mode converter can reach a broadband working range as well as a high conversion efficiency, which shows a great potential in optical communication systems and some other areas. The combining of chirp and cascading don't increase the difficulty of fabrication. What's more, the way we design the mode converter doesn't have any special demand on the structure designing or dispersion properties of fiber.

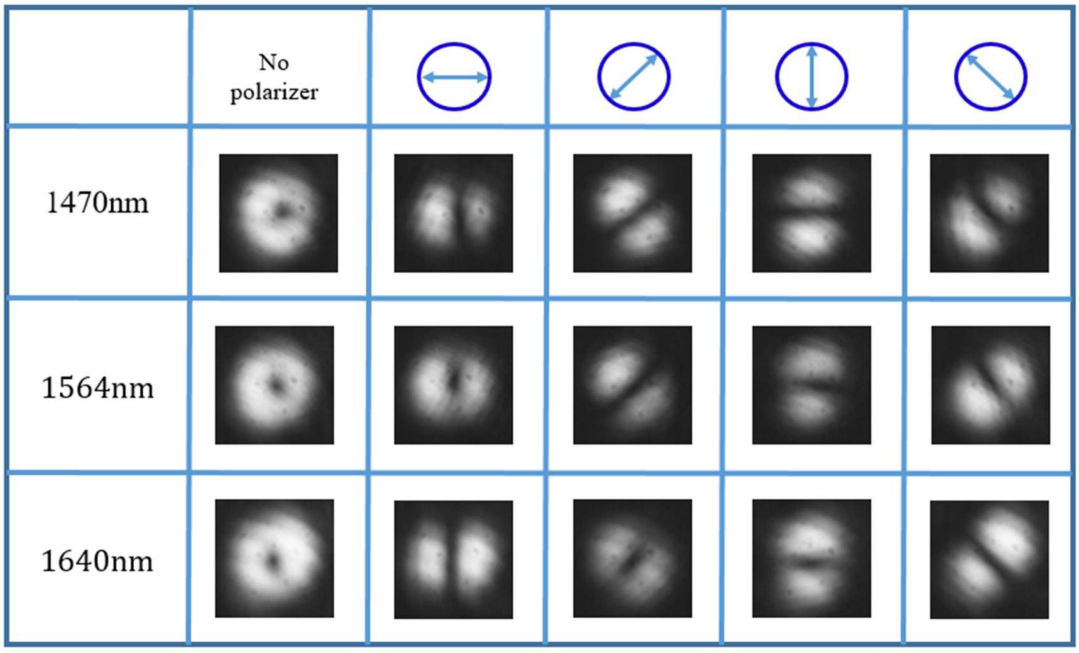

Fig. 11. Intensity profile of the HE_{21}^{even} mode at different wavelength.

4. Conclusions

We have demonstrated a new way to realize an ultra-broadband mode conversion by cascading chirped long-period fiber grating. In simulation part, we analyzed the effects of each parameter on the designed CLPFG and get a 20 dB bandwidth of 145 nm from 1485 nm to 1630 nm, as well as a 10 dB bandwidth of 170 nm from 1472 nm to 1642 nm when $\Delta d = 5$, $N = 4$ and $\kappa = 551\ m^{-1}$. In the meantime, experimental results are in good agreement with the theoretical simulation and finally we got a CLPFG whose 10 dB bandwidth is 170 nm from 1470 nm to 1640 nm, and 13 dB bandwidth is 145 nm from 1487 nm to 1632 nm. This mode-conversion device provides a convenient way to realize a tunable broadband mode conversion operation and could be used in optical tweezers, high-resolution imaging, surface plasmon excitation, optical data transmission, and material processing.

References

[1] J. M. Dudley, F. Dias, M. Erkintalo, and G. Genty, "Instabilities, breathers and rogue waves in optics," *Nature Photon.*, vol. 8, no. 10, pp. 755–764, Oct. 2014.
[2] R. J. Essiambre, G. Kramer, P. J. Winzer, G. J. Foschini, and B. Goebel, "Capacity limits of optical fiber networks," *J. Lightw. Technol.*, vol. 28, no. 4, pp. 662–701, Feb. 15, 2010.
[3] G. C. Valley, "Photonic analog-to-digital converters," *Opt. Express*, vol. 15, no. 5, pp. 1955–1982, Mar. 5, 2007.
[4] G. A. Mourou *et al.*, "Exawatt-Zettawatt pulse generation and applications," *Opt. Commun.*, vol. 285, no. 5, pp. 720–724, Mar. 1, 2012.
[5] N. Bozinovic *et al.*, "Terabit-scale orbital angular momentum mode division multiplexing in fibers," *Science*, vol. 340, no. 6140, pp. 1545–1548, Jun. 28, 2013.
[6] P. Gregg, P. Kristensen, and S. Ramachandran, "13.4 km OAM state propagation by recirculating fiber loop," *Opt. Express*, vol. 24, no. 17, pp. 18938–18947, Aug. 22, 2016.
[7] Y. Yue *et al.*, "1.6-Tbit/s muxing, transmission and demuxing through 1.1-km of vortex fiber carrying 2 OAM beams each with 10 wavelength channels," in *Proc. Opt. Fiber Commun. Conf. Expo. Nat. Fiber Optic Eng. Conf.*, 2013, Paper OTh4G.2.
[8] M. Salsi *et al.*, "Mode-division multiplexing of 2 x 100 Gb/s channels using an LCOS-based spatial modulator," *J. Lightw. Technol.*, vol. 30, no. 4, pp. 618–623, Feb. 15, 2012.

[9] W. Wang, J. Wu, K. Chen, W. Jin, and K. S. Chiang, "Ultra-broadband mode converters based on length-apodized long-period waveguide gratings," *Opt. Express*, vol. 25, no. 13, pp. 14341–14350, Jun. 26, 2017.
[10] W. Jin and K. S. Chiang, "Mode converters based on cascaded long-period waveguide gratings," *Opt. Lett.*, vol. 41, no. 13, pp. 3130–3133, Jul. 1, 2016.
[11] X. P. Liu, R. M. Osgood, Y. A. Vlasov, and W. M. J. Green, "Mid-infrared optical parametric amplifier using silicon nanophotonic waveguides," *Nature Photon.*, vol. 4, no. 8, pp. 557–560, Aug. 2010.
[12] K. K. Xu *et al.*, "Light emission from a poly-silicon device with carrier injection engineering," *Mater. Sci. Eng. B-Adv. Functional Solid-State Mater.*, vol. 231, pp. 28–31, May 2018.
[13] X. Zhang, Y. Liu, Z. Wang, J. Yu, and H. Zhang, "LP01-LP11a mode converters based on long-period fiber gratings in a two-mode polarization-maintaining photonic crystal fiber," *Opt. Express*, vol. 26, no. 6, pp. 7013–7021, Mar. 19, 2018.
[14] Y. H. Zhao, Y. Q. Liu, L. Zhang, C. Y. Zhang, J. X. Wen, and T. Y. Wang, "Mode converter based on the long-period fiber gratings written in the two-mode fiber," *Opt. Express*, vol. 24, no. 6, pp. 6186–6195, Mar. 21, 2016.
[15] A. B. Taher *et al.*, "Adiabatically tapered microstructured mode converter for selective excitation of the fundamental mode in a few mode fiber," *Opt. Express*, vol. 24, no. 2, pp. 1376–1385, Jan. 25, 2016.
[16] G. Pelegrina-Bonilla, K. Hausmann, H. Sayinc, U. Morgner, J. Neumann, and D. Kracht, "Analysis of the modal evolution in fused-type mode-selective fiber couplers," *Opt. Express*, vol. 23, no. 18, pp. 22977–22990, Sep. 7, 2015.
[17] H. Wu *et al.*, "All-fiber second-order optical vortex generation based on strong modulated long-period grating in a four-mode fiber," *Opt. Lett.*, vol. 42, no. 24, pp. 5210–5213, Dec. 15, 2017.
[18] I. Giles, A. Obeysekara, R. S. Chen, D. Giles, F. Poletti, and D. Richardson, "Fiber LPG mode converters and mode selection technique for multimode SDM," *IEEE Photon. Technol. Lett.*, vol. 24, no. 21, pp. 1922–1925, Nov. 1, 2012.
[19] Y. Han *et al.*, "Controllable all-fiber generation/conversion of circularly polarized orbital angular momentum beams using long period fiber gratings," *Nanophotonics*, vol. 7, no. 1, pp. 287–293, Jan. 2018.
[20] J. L. Dong and K. S. Chiang, "Temperature-insensitive mode converters with CO2-laser written long-period fiber gratings," *IEEE Photon. Technol. Lett.*, vol. 27, no. 9, pp. 1006–1009, May 1, 2015.
[21] Y. C. Guo, Y. G. Liu, Z. Wang, Z. H. Wang, and H. W. Zhang, "All-fiber mode-locked cylindrical vector beam laser using broadband long period grating," *Laser Phys. Lett.*, vol. 15, no. 8, Aug. 2018, Art. no. 085108.
[22] Y. Guo *et al.*, "More than 110-nm broadband mode converter based on dual-resonance coupling mechanism in long period fiber gratings," *Opt. Laser Technol.*, vol. 118, pp. 8–12, 2019.
[23] S. Ramachandran *et al.*, "All-fiber grating-based higher order mode dispersion compensator for broad-band compensation and 1000-km transmission at 40 Gb/s," *IEEE Photon. Technol. Lett.*, vol. 13, no. 6, pp. 632–634, Jun. 2001.
[24] S. Ramachandran, S. Ghalmi, Z. Y. Wang, and M. Yan, "Band-selection filters with concatenated long-period gratings in few-mode fibers," *Opt. Lett.*, vol. 27, no. 19, pp. 1678–1680, Oct. 1, 2002.
[25] B. R. Acharya, T. Krupenkin, S. Ramachandran, Z. Wang, C. C. Huang, and J. A. Rogers, "Tunable optical fiber devices based on broadband long-period gratings and pumped microfluidics," *Appl. Phys. Lett.*, vol. 83, no. 24, pp. 4912–4914, Dec. 15, 2003.
[26] Z. Y. Wang and S. Ramachandran, "Ultrasensitive long-period fiber gratings for broadband modulators and sensors," *Opt. Lett.*, vol. 28, no. 24, pp. 2458–2460, Dec. 15, 2003.
[27] S. Ramachandran, Z. Y. Wang, and M. Yan, "Bandwidth control of long-period grating-based mode converters in few-mode fibers," *Opt. Lett.*, vol. 27, no. 9, pp. 698–700, May 1, 2002.
[28] D. Ostling and H. E. Engan, "Broadband spatial mode conversion by chirped fiber bending," *Opt. Lett.*, vol. 21, no. 3, pp. 192–194, Feb. 1, 1996.
[29] H. Ke, K. S. Chiang, and J. H. Peng, "Analysis of phase-shifted long-period fiber gratings," *IEEE Photon. Technol. Lett.*, vol. 10, no. 11, pp. 1596–1598, Nov. 1998.
[30] J. Yao, L. Zhan, Y. X. Wang, H. G. Li, S. Y. Luo, and Y. X. Xia, "Femtosecond pulse delivery using a chirped long-period grating of multi-mode fiber for mode conversion," *J. Modern Opt.*, vol. 57, no. 6, pp. 485–491, 2010.
[31] G. Volpe, G. P. Singh, and D. Petrov, "Optical tweezers with cylindrical vector beams produced by optical fibers," *Opt. Trapping Opt. Micromanipulation*, vol. 5514, pp. 283–292, 2004.
[32] L. Novotny, M. R. Beversluis, K. S. Youngworth, and T. G. Brown, "Longitudinal field modes probed by single molecules," *Physical Rev. Lett.*, vol. 86, no. 23, pp. 5251–5254, Jun. 4, 2001.
[33] A. Bouhelier *et al.*, "Surface plasmon interference excited by tightly focused laser beams," *Opt. Lett.*, vol. 32, no. 17, pp. 2535–2537, Sep. 1, 2007.
[34] D. Lin *et al.*, "Efficient, high-power, and radially polarized fiber laser," *Opt. Lett.*, vol. 35, no. 13, pp. 2290–2292, Jul. 1, 2010.
[35] K. K. Xu, "Monolithically integrated Si gate-controlled light-emitting device: Science and properties," *J. Opt.*, vol. 20, no. 2, Feb. 2018, Art. no. 024014.
[36] H. W. Zhang, Y. G. Liu, Z. Wang, B. W. Mao, Y. Han, and K. Yang, "Generation of arbitrary polarized OAM mode based on a fiber mode selective coupler," *J. Opt.*, vol. 21, no. 8, Aug. 2019, Paper 085705.
[37] F. Y. M. Chan and K. S. Chiang, "Analysis of apodized phase-shifted long-period fiber gratings," *Opt. Commun.*, vol. 244, no. 1-6, pp. 233–243, Jan. 3, 2005.
[38] W. Huang *et al.*, "Multi-component-intermodal-interference mechanism and characteristics of a long period grating assistant fluid-filled photonic crystal fiber interferometer," *Opt. Express*, vol. 22, no. 5, pp. 5883–5894, Mar. 10, 2014.
[39] R. Magnusson and M. Shokooh-Saremi, "Physical basis for wideband resonant reflectors," *Opt. Express*, vol. 16, no. 5, pp. 3456–3462, Mar. 3, 2008.
[40] K. K. Xu, "Silicon MOS optoelectronic micro-nano structure based on reverse-biased PN junction," *Physica Status Solidi a-Appl. Mater. Sci.*, vol. 216, no. 7, Apr. 10, 2019, Paper 1800868.
[41] B. L. Bachim and T. K. Gaylord, "Polarization-dependent loss and birefringence in long-period fiber gratings," *Appl. Opt.*, vol. 42, no. 34, pp. 6816–6823, Dec. 1, 2003.